Electronic structure of $In_yGa_{1-y}As_{1-x}N_x$/GaAs multiple quantum wells in the dilute-*N* regime from pressure and k·p studies

S. A. Choulis,* T. J. C. Hosea, S. Tomić, M. Kamal-Saadi, A. R. Adams, and E. P. O'Reilly[†]
Department of Physics, University of Surrey, Guildford, Surrey GU2 7XH, UK

B. A. Weinstein[‡]
Department of Physics, SUNY at Buffalo, Buffalo, New York 14260

P. J. Klar
Department of Physics and Materials Science Center, Philipps-University, D-35032 Marburg, Germany
(Received 22 March 2002; published 30 October 2002)

We report photomodulated reflectance measurements of several intersubband transitions for a series of as-grown $In_yGa_{1-y}As_{1-x}N_x$/GaAs multiple quantum well samples as functions of hydrostatic pressure (at room temperature) and temperature (at ambient pressure). The experimental results provide support for the effects of disorder due to different nearest-neighbor N-cation configurations. The quantum well transition energies obtained from the photomodulated reflectance spectra are fitted as a function of pressure with a realistic 10 band **k**·**p** Hamiltonian, that includes tight-binding-based energies and coupling parameters for the N levels. The quality of match between theory and experiment confirms the theoretical model and predicts some important material parameters for dilute-N InGaAsN alloys.

DOI: 10.1103/PhysRevB.66.165321 PACS number(s): 78.20.Ci, 71.20.Nr, 62.50.+p

I. INTRODUCTION

Recent work has shown that the substitution of dilute amounts of nitrogen at anion sites in certain group III-V semiconductors dramatically reduces the fundamental bandgap (see note added) and increases the electron mass compared to the host material. These modifications result from the ability of N to form isoelectronic impurity states that, while spatially localized, are resonant with the conduction band (CB) and strongly coupled to the extended CB states.[1–9] In a simplified picture, the N-CB interaction repels the CB edge and decreases the CB curvature, which, in turn, causes the pressure dependence of the fundamental bandgap to be unusually weak and nonlinear.[1,2] This pressure behavior is an identifying characteristic of the N-CB interaction, and can be used to investigate the interaction strength. Useful **k**·**p**-like parametrizations of the band structure can be made based on the level repulsion model introduced by Shan *et al.*[1] The novel bandstructure properties of dilute-N III-V alloys offer attractive opportunities for improved device engineering in infrared optoelectronic applications, and several promising advances have been reported recently for 1.3–1.55 μm laser structures that employ this intriguing class of alloy materials.[10–13]

The present paper uses photomodulated reflectance (PR) spectroscopy to explore the pressure and temperature dependences of the intersubband transitions in laser-prototype $In_yGa_{1-y}As_{1-x}N_x$/GaAs ($0 \leqslant x \leqslant 4.3\%$) multiple quantum well (MQW) samples. These dependences are found to weaken with increasing N content, in accord with other experimental and theoretical results on a variety of dilute-N III-V systems.[1,8,14–18] However, it was evident in earlier work that broadening of the PR spectra indicated the presence of important N-related disorder effects.[14] Here, we seek to gain a more comprehensive picture of the influence of nitrogen on the confined levels in $In_yGa_{1-y}As_{1-x}N_x$/GaAs MQWs, including the effects of disorder due to different nearest-neighbor N-cation configurations. A 10-band **k**·**p** model, with parameters derived from tight-binding supercell calculations, is employed to analyze our pressure data. Reliable semiempirical results are obtained for the effect of N content on the CB offset and the electron effective mass, as functions of pressure in this system. The present findings are important, both for progress in developing InGaAsN-based QW devices, and for advancing the general understanding of the N-CB interaction in III-V-N dilute alloys.

II. EXPERIMENTAL CONSIDERATIONS

We studied four compressively strained $In_yGa_{1-y}As_{1-x}N_x$/GaAs MQW samples having N and In contents x and y, respectively, in the ranges $0 \leqslant x \leqslant 0.043$ and $0.25 \leqslant y \leqslant 0.32$, with well and barrier widths between 85–150 Å. The specific composition and structural parameters of our samples are listed in Table I. The samples were grown by metal-organic vapor phase epitaxy (MOVPE) on buffered semi-insulating GaAs (001) substrates, and were characterized by standard x-ray rocking curve and transmission elec-

TABLE I. Compositions and structural information for the four samples studied in this work.

Sample	In conc. (%)	N conc. (%)	Well width (nm)	Barrier width (nm)
1	25 ± 2	0	13.5 ± 0.5	93 ± 0.5
2	32 ± 2	0.3 ± 0.1	14.6 ± 0.5	13 ± 0.5
3	28 ± 2	2.5 ± 0.3	8.9 ± 0.5	10 ± 0.5
4	30 ± 2	4.3 ± 0.5	8.9 ± 0.5	13 ± 0.5

 ©2002 The American Physical Society

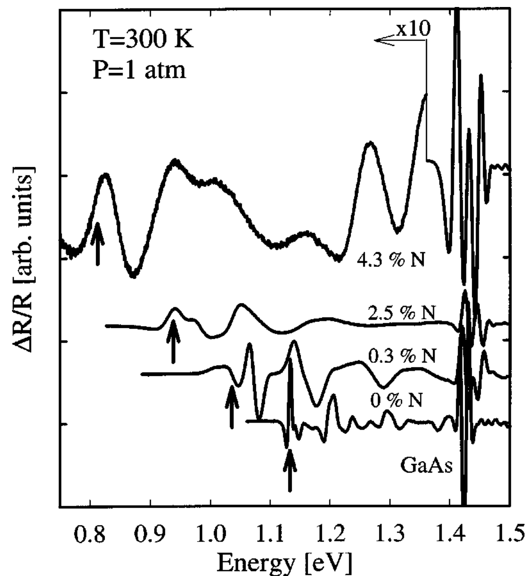

FIG. 1. Room-temperature ambient pressure PR spectra for the $In_yGa_{1-y}As_{1-x}N_x$/GaAs MQW samples (Table I). The arrows indicate the effective band gap in each sample (obtained by subsequent least-squares fitting).

tron microscopy methods.[19] The N-free sample has five QWs, while all the other samples have three QWs. The cryogenic studies were performed in the range 300–10 K at ambient pressure (1 atm) using a conventional closed-cycle He refrigerator. The pressure experiments were carried out up to 86 kbar at 300 K using a diamond-anvil cell with an alcohol pressure medium. The applied hydrostatic pressure is calibrated by both the standard ruby method, and by the shift of the bulk GaAs bandgap in the samples' substrate and barrier regions (which appears as a sharp PR feature up to ~55 kbar, somewhat above the GaAs Γ-X crossover). More details about the experimental procedures can be found elsewhere.[14]

III. PHOTOMODULATED REFLECTANCE RESULTS

Figure 1 shows the PR spectra observed at ambient pressure (1 atm) and room temperature for the four samples studied. The arrows indicate the effective band gap for each sample (obtained by least-squares fitting—see later). Examination of the data clearly reveals two trends as a function of increasing N content: (i) a rapid redshift in the transition energies and (ii) a strong broadening in the line shapes.

The redshift is caused by the N-CB interaction. The bandgap shift is ~0.08 eV per N at. %, which is slightly smaller than the results found in prior studies on thick $In_yGa_{1-y}As_{1-x}N_x$ epilayers[1] and on a variety of dilute-N III-V MQWs.[15,20,21] As expected, the E_+ transition reported at ~1.7–1.8 eV (depending on the N and In content) in thick epilayer systems,[1] could not be observed in our MQW samples despite a careful examination of the relevant spectral region. To our knowledge, the E_+ transition has not been seen so far in any dilute-N quantum well systems.

The line-shape broadening seen in Fig. 1 is a strong indication of the presence of increasing intrinsic disorder in the QW layers with greater N content. Disorder effects—arising from defects, nonuniform strain, and fluctuations in the density and arrangement of In and N—are well known in MOVPE-grown epitaxial InGaAsN having N contents exceeding a few tenths of an at. %.[22,23] Furthermore, the present samples were not subjected to any post-growth annealing to lower the disorder closer to what would be present for thermal equilibrium growth conditions.

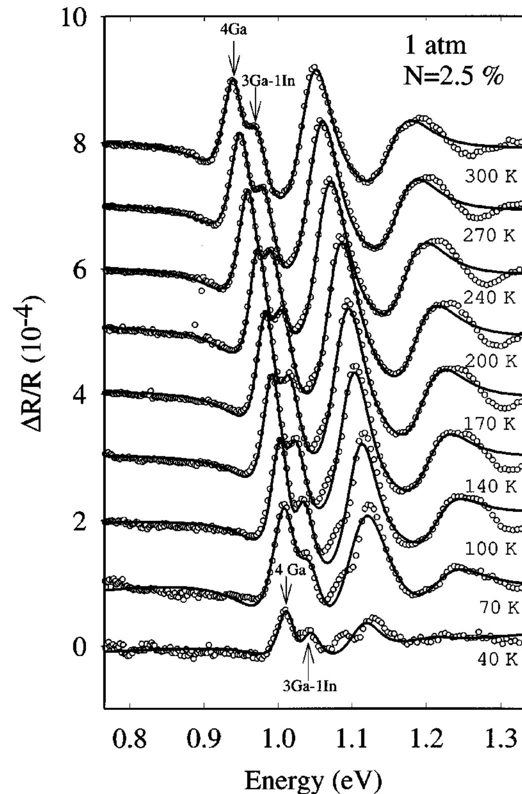

FIG. 2. Effect of temperature on the observed PR spectra at 1 atm (circles) for the sample having 2.5% N content in the QWs, and multioscillator fits to the spectra (solid curves). The arrows indicate the low-energy doublet corresponding to N bound to either 4 Ga, or 1In-3Ga, nearest neighbors (see text).

Figures 2 and 3 show the PR spectra of the sample containing 2.5% N for several temperatures between 40–300 K (1 atm) and several pressures between 0–86 kbar (300 K), respectively. In these data, the transition energies are deduced as functions of temperature and pressure from multioscillator representations of the observed spectra (points) by finding the best-fit (solid curves) to a sum of Aspnes-type third differential line shapes.[24] Then the fitted oscillators are identified by comparison to the transitions predicted in the 10-band $\mathbf{k}\cdot\mathbf{p}$ calculations described below. Table II gives these assignments. For the sample containing 4.3% N, we find that its weak signal and broadening are too severe to allow this analysis to be performed in a meaningful way, and consequently the results for this sample have not been included in Table II.

An examination of the PR spectra in Fig. 1 for the samples containing 0.3 and 2.5 % N shows that the broadening in the lowest energy transition (i.e., the effective QW bandgap) is caused in large part by the presence of a doublet

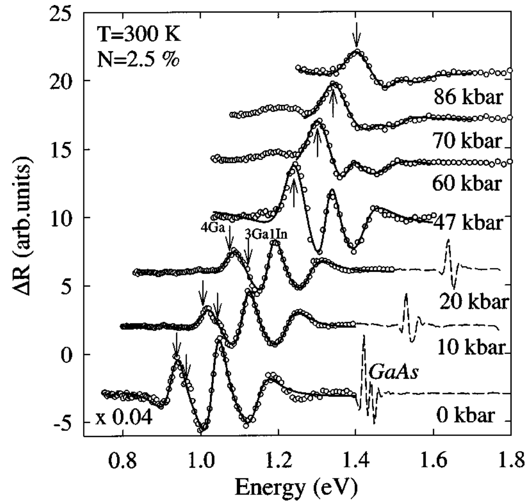

FIG. 3. Effect of pressure on the observed PR spectra at 300 K (circles and dashed curves) for the sample having 2.5% N content in the QWs and multioscillator fits (solid curves). The arrows again indicate the low-energy doublet feature attributed to cation disorder, which can be observed up to 20 kbar.

structure. Although one might, at first sight, suspect that heavy-hole–light-hole splitting is a possible explanation for the origin of this low-energy structure, we have found that its two components cannot be modeled successfully as a function of pressure and N content in this way. In Figs. 2 and 3, the doublet structure is observed clearly for all temperatures between 300–40 K (at 1 atm), and for pressures up to 20 kbar (at 300 K). The splitting does not depend significantly on temperature (within our experimental uncertainty), but it increases from ~25–30 meV at 1 atm to ~40–45 meV at 20 kbar. Above this pressure, the two features can no longer be resolved because of a general increase in the spectral broadening, and a decrease in the strength of the doublet's high-energy component.

Based on the results of recent tight-binding atomic-cluster calculations,[25] we attribute this low-energy doublet to the effects of variations in the N-cation nearest-neighbor configuration in the InGaAsN alloy. For the ranges of In content (28–30 %) and N content (0.3 and 2.5 %) in the samples that show the doublet, fluctuations in the number of Ga and In neighbors around different N sites are expected to produce important disorder effects on the CB edge.[25,26] In this interpretation, the low-energy doublet reflects density-of-states structure in a disorder-induced band tail derived from the QWs lowest confined electron level. As is common in PR, the higher order transitions are more broadened, which here tends to obscure the effects of the different configurations in the associated spectral features.[25] We assign the lower-energy feature in the doublet (see Figs. 2 and 3) to transitions in regions where N atoms are predominantly bonded to four Ga atoms, and the higher-energy one to regions where the average N-atom environment is closer to 3 Ga and 1 In bonds. This assignment is in accord with the predictions of the tight-binding results,[25] which show that the energy-order assigned here for the N-4Ga and N-(3Ga,1In) levels results from a weakening of the N-CB interaction (V_{Nc}, see next section) for higher numbers of N-In nearest-neighbor

TABLE II. Summary of the three samples studied, showing the assignments of the QW transitions and the results from fitting the associated PR spectra as a function of pressure (at 300 K) and temperature (at 1 atm). The first column gives our final assignments of the observed transitions, based on the ten-band $\mathbf{k}\cdot\mathbf{p}$ calculations. The next two columns give the linear and quadratic pressure coefficients of the observed transition energies, obtained by least-square data fits using $E(P)=E_0+aP+bP^2$ (not shown in Fig. 4). The last three columns describe the best-fit temperature dependence (at 1 atm) of the observed PR transitions in terms of the Bose-Einstein expression $E(T)=E_B-\alpha_B[1+2/(e^{\Theta/T}-1)]$.

Assignment based on calculations	E (eV) 1 atm, 300 K ±0.015	a (eV/kbar) ±0.5	b (eV/kbar^2) $\pm 2.0\times10^{-5}$	E_B (eV) 1 atm	α_B (meV)	Θ (K)
Sample 1 (0% N)						
e_3-hh_3	1.296	11.4×10^{-3}	-5.1×10^{-5}			
e_1-lh_1	1.229	11.1×10^{-3}	-4.4×10^{-5}			
e_2-hh_2	1.200	10.5×10^{-3}	-3.6×10^{-5}	1.280	35.53	183.19
e_1-hh_1	1.134	10.4×10^{-3}	-3.2×10^{-5}	1.214	35.53	183.19
Sample 2 (0.3% N)						
e_1-lh_1	1.138	8.4×10^{-3}	-2.9×10^{-5}	1.231	44.99	219.84
e_2-hh_2/e_1-hh_3	1.066	8.5×10^{-3}	-2.9×10^{-5}	1.158	44.99	219.84
e_1-hh_1	1.034	8.5×10^{-3}	-4.0×10^{-5}	1.112	44.99	219.84
Sample 3 (2.5% N)						
e_1-VB	1.149	6.5×10^{-3}	-1.8×10^{-5}	1.233	48.76	253.40
e_1-lh_1	1.043	7.3×10^{-3}	-2.6×10^{-5}	1.120	48.76	253.40
e_1-hh_1	0.941	7.8×10^{-3}	-2.7×10^{-5}	1.010	48.76	253.40

bonds.[25,26] This is also consistent with the observed increase in the doublet splitting with pressure, since a larger V_{Nc} value would also increase the quadratic (sublinear) term in the pressure shift of the N-4Ga level compared to the more In-rich nearest-neighbor environments. Such assignments are in accord with Ref. 27, where it was shown by FTIR vibrational spectroscopy that annealing converts the environment of N from 4 Ga to 3Ga-1In. Furthermore, the assignments are in good agreement with our recent work on an InGaAsN vertical-cavity surface-emitting laser structure, where the different N configurations broaden the gain spectrum and allow the laser to operate over an unusually wide temperature range.[28]

IV. THEORETICAL TEN-BAND k·p MODEL OF $In_yGa_{1-y}As_{1-x}N_x$/GaAs QWs

We use a ten-band $\mathbf{k}\cdot\mathbf{p}$ Hamiltonian to calculate the QW confined-state energies, and their pressure dependence. The basis states (which each are doubly spin degenerate) include the highest valence bands (i.e., heavy hole, light hole, and spin-orbit split off) and the lowest CB of the $In_yGa_{1-y}As$ host material at $\mathbf{k}=0$, and an additional pair of basis states representing the nitrogen resonant level. This Hamiltonian structure has been found to give an excellent account of the measured band-edge properties in bulk $In_yGa_{1-y}As_{1-x}N_x$, including the effects on the bandgap and the CB mass of variations in the N and In contents, and variations in the applied (or internal) strain.[29] It also has been applied successfully to predict the gain characteristics of dilute-nitride QW lasers.[11,30,31] The ten-band $\mathbf{k}\cdot\mathbf{p}$ Hamiltonian is further justified by comparison of the energy-band dispersion that it predicts with that *calculated* using the tight-binding supercell approach, where, with a reasonable choice of the $\mathbf{k}\cdot\mathbf{p}$ parameters, one obtains excellent agreement for the lowest CB until at least 200 meV above the CB edge.[7]

We quantize the Hamiltonian along the growth direction (z axis), perpendicular to the growth plane. For zero in-plane momentum ($k_x=k_y=0$), the 10×10 $\mathbf{k}\cdot\mathbf{p}$ Hamiltonian decouples into two independent 5×5 Hamiltonians H which we can use to determine the band edge energies in InGaNAs heterostructures:

$$H=\begin{pmatrix} E_{\mathrm{N}} & V_{Nc} & 0 & 0 & 0 \\ V_{Nc}^{*} & E_{\mathrm{CB}} & 0 & \sqrt{2}U & U \\ 0 & 0 & E_{\mathrm{HH}} & 0 & 0 \\ 0 & \sqrt{2}U^{*} & 0 & E_{\mathrm{LH}} & Q \\ 0 & U^{*} & 0 & Q^{*} & E_{\mathrm{SO}} \end{pmatrix} \tag{1}$$

where the subscripts N, CB, HH, LH, and SO stand for nitrogen-resonant, conduction band, heavy-hole, light-hole, and split-off bands respectively; V_{Nc} describes the interaction between the N state and the CB edge, U the mixing between the conduction and valence bands (VBs) at finite k_z, and Q the mixing between the light-hole and split-off bands at finite k_z and strain. Because of the difference between the InGaNAs and the GaAs lattice constants, the InGaNAs QWs are generally under biaxial strain. The matrix elements in Eq. (1) are determined as functions of N composition x, In composition y, in-plane strain ε_{xx}, and applied hydrostatic pressure P, as detailed in the Appendix.

As already remarked, calculations in QWs composed of InGaAsN quaternary alloys are complicated by cation disorder. A substitutional N atom on an As site can be surrounded by five different configurations of nearest-neighbor cations $Ga_{\xi}In_{4-\xi}$ ($\xi=4,3,2,1,0$). Hence, there are five different values for the N level E_{N}, and five corresponding values for the interaction V_{Nc} between these resonant N states and the CB edge. To simplify the present numerical treatment at *high pressure*, we use values of E_{N} and V_{Nc} that average the different ξ cases—in effect fitting the eigenvalues obtained from the $\mathbf{k}\cdot\mathbf{p}$ Hamiltonian to the mean energies of QW levels that are broadened by cation disorder. Thus we use a virtual crystal approximation to describe the N nearest-neighbor environment. The coupling parameter V_{Nc} between the N resonant level and the CB edge is assumed to be independent of pressure and to vary with N composition x as $V_{Nc}=1.675\sqrt{x}$ eV. We also take the energy separation between the nitrogen level and the bottom of the CB to be independent of In composition in unstrained InGaNAs, $\Delta E_{Nc}(p=0)=0.485$ eV. Although there are many uncertainties in the analysis used here, we have sought to ensure that all the parameter values employed are consistent with the available theoretical and experimental data. In addition, we have purposely fitted the PR spectra with the *minimum* number of oscillators needed to represent the major observed features (consistent with the thickness and barrier height of the QWs). Hence, while the temperature-dependent PR results show four oscillators in all spectra (Fig. 2), in the pressure-dependent data the lowest two are resolvable only up to 20 kbar (see the solid curves in Fig. 3), which is why we choose to fit the whole set of latter spectra with only three oscillators.

V. RESULTS AND DISCUSSION

The predictions of the above calculations are put to a stringent test by our pressure results on $In_yGa_{1-y}As_{1-x}N_x$/GaAs MQWs. This is because the data provide a relatively large number of confined interband transitions, each of which must be fit by a *self-consistent set* of model parameters for different pressures, N content, In content, and well/barrier dimensions—with the pressure and N content varying over considerable ranges. These parameters are constrained within realistic limits, as described above. An optimized semiempirical fit to the observed pressure dependence of the interband energies is then computed by allowing the sample compositions and dimensions to vary only inside the uncertainties set by growth conditions (see Table I), with standard minor-scaling of the other $\mathbf{k}\cdot\mathbf{p}$ parameters, as appropriate.

The results of this analysis are summarized in Fig. 4 for the three samples having N contents of 0–2.5 %. The solid curves represent the computed optimized $\mathbf{k}\cdot\mathbf{p}$ fits to the measured transition energies (points) for pressures up to 70 kbar. The main part of the figure focuses on the lowest energy oscillator in each sample, assigned to e_1-hh_1—essentially

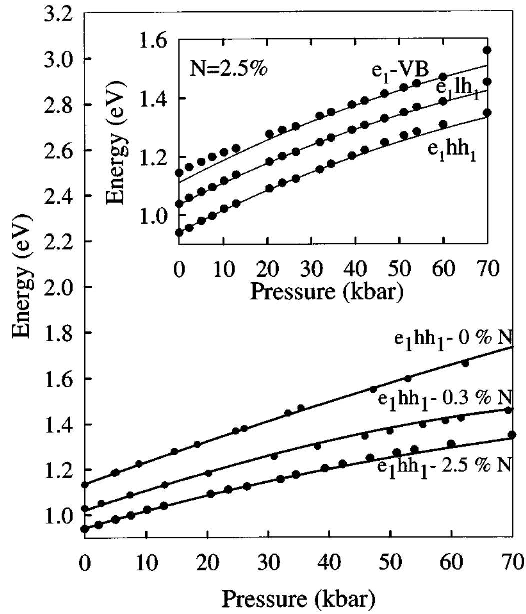

FIG. 4. Observed pressure dependence of the e_1-hh_1 transition (filled circles) for the samples having N contents of 0, 0.3, and 2.5 % in the QWs. Solid curves are calculated using the optimized ten-band $\mathbf{k}\cdot\mathbf{p}$ model. The inset shows the measured and calculated pressure dependence for the three observed interband oscillators in the 2.5% N sample.

the effective QW bandgap broadened by cation disorder. The inset shows the pressure dependence for all three of the observed transitions in the 2.5% N-content sample. These transitions are assigned to e_1-hh_1, e_1-lh_1, and e_1-VB (i.e., cross interface to the barrier's VB edge.) Our attempts at alternative assignments substantially degraded the agreement. For example, the e_1-VB feature might also contain contributions from other normally forbidden or weak off-diagonal transitions, such as e_1-hh_3 or e_2-lh_1, but these choices provided a significantly poorer overall fit to the data.

Table II gives the linear and quadratic pressure coefficients of the observed transition energies in Fig. 4, obtained by least-square fits to the data points with expressions of the form $E=E_0+aP+bP^2$ (not shown in Fig. 4). Note that the pressure dependence of the VB offset can be estimated for the 2.5%-N sample from the results in the inset to Fig. 4. The observed linear pressure coefficients a in Table II suggest a marginal decrease in this offset, between the 0 and 2.5 % N samples, of $\sim -1\pm1$ meV/kbar for pressures up to 20 kbar, an interesting finding that merits further experimental and theoretical study.

The close agreement between theory and experiment in Fig. 4 indicates that our ten-band $\mathbf{k}\cdot\mathbf{p}$ analysis, tight-binding-based N parameters, and conventional InGaAs parameters give a successful description of the effects of the interaction between resonant N states and the $In_yGa_{1-y}As$ host CB in the QWs. We find, as suggested by Shan *et al.*,[1] that the repulsion between the s-like CB edge and the A_1 symmetry N level gives rise to linear pressure coefficients for the interband transitions that are intermediate between that of the host bandgap (essentially e_1-hh_1 in our 0% N sample) and that of the N impurity level. The same mechanism explains the large sublinear dependence of the pressure shifts in N-containing MQW samples, since the repulsion between the CB edge and E_N increases as pressure reduces the separation between these levels. The calculated results reproduce the details of this behavior in the QWs under conditions in which the mismatch strain, band offset, and electron effective mass, vary with pressure by nontrivial amounts.

The effect of the interaction between the CB states and the N-resonant band is also clear in our temperature results. The transition energies are well described as a function of temperature by fitted Bose-Einstein expressions (see Table II). The temperature behavior of the effective band gap observed in the PR data was also confirmed using photoluminescence measurements. The Bose-Einstein parameters α_B and Θ are assumed to be the same for different transitions within a given sample, but to differ from sample to sample. The parameter Θ is proportional to the average frequency of the phonons, and, so, should increase with N content. Considering that α_B is the difference between the actual effective bandgap at $T=0$ K, and the $T=0$ K intercept of the bandgap's linear asymptote at very high T, the values of α_B in Table II indicate that the bandgap renormalization effect decreases with increasing N content. From the Bose-Einstein expression we get a total shift from 0–300 K of ~84 meV for the 0% sample, and ~83 meV (viz., marginally less) and ~73 meV for the 0.3 and 2.5 % samples, respectively. Hence, the total variation of the observed QW transition energies between 0 and 300 K is slightly reduced by the N content. Essentially this is in agreement with other observations of the effects of N on the temperature-induced shift of the absorption edge—reported to be reduced by 12% in InGaAsN bulk alloys with N= 1.5% (Ref. 32) and by 40% in GaNAs bulk alloys with $N>1\%$.[33] Note that the effects of low temperature and high pressure are similar. We attribute this to the fact that, in both cases, the CB edge moves closer to the N level, and thus the Γ character of the CB edge is modified by mixing with the localized N level.

The effects of applied pressure on the electron effective mass and the CB offset are explored further in Figs. 5 and 6. These results are calculated for the samples with N contents of 0, 0.3, and 2.5 % using the optimized ten-band $\mathbf{k}\cdot\mathbf{p}$ model. Figure 5 gives the pressure dependence of the density-of-states effective mass[34] obtained from the dispersion at the CB edge in appropriately strained $In_yGa_{1-y}As_{1-x}N_x$, evaluated at the energy of the e_1 confinement level and for $\mathbf{k}_{\text{in plane}}=0$. In order to explain the influence of pressure on m_e^*, one needs to consider two competing effects: (i) The decrease in the bandgap with increasing N content tends to reduce the electron mass, as in conventional semiconductors (i.e., $\Delta m_e^*/m_e^* \approx \Delta E_g/E_g$), (ii) the repulsive N-CB interaction tends to flatten the CB, and so increase m_e^*. At very low N content and ambient pressure, this competition weakly favors the bandgap effect. The calculated electron mass for the different samples decreases, initially, with increasing N content—falling from $0.055m_0$ for $x=0\%$ to $0.053m_0$ for $x=0.3\%$, mainly due to the significant effect on the bandgap of the 7% increase in In content for the 0.3% N sample. However, with further increase in the N content to

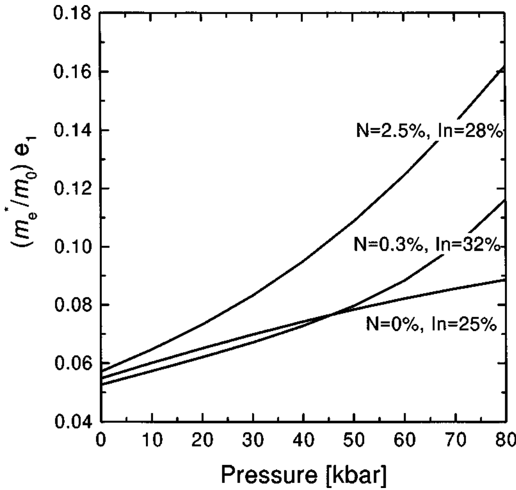

FIG. 5. Predicted pressure dependence of the electron effective mass for the e_1 quantum level in the MQW samples containing 0, 0.3, and 2.5% N content, as calculated using the optimized ten-band $\mathbf{k}\cdot\mathbf{p}$ model.

$x=2.5\%$ (despite the 3% increase in the In content compared to the N-free sample, see Table I), the calculated mass rises to $0.057m_0$ as the N-CB interaction, i.e., the effect of $V_{Nc} \sim\beta\sqrt{x}$ becomes dominant. Under high pressure, *both mechanisms promote a heavier effective mass*, since pressure increases the $In_yGa_{1-y}As_{1-x}N_x$ bandgap and, at the same time, reduces the energy separation between E_N and the CB edge. Hence, m_e^* increases with pressure in all three QW samples, but the change is stronger for higher N content because V_{Nc} is larger.

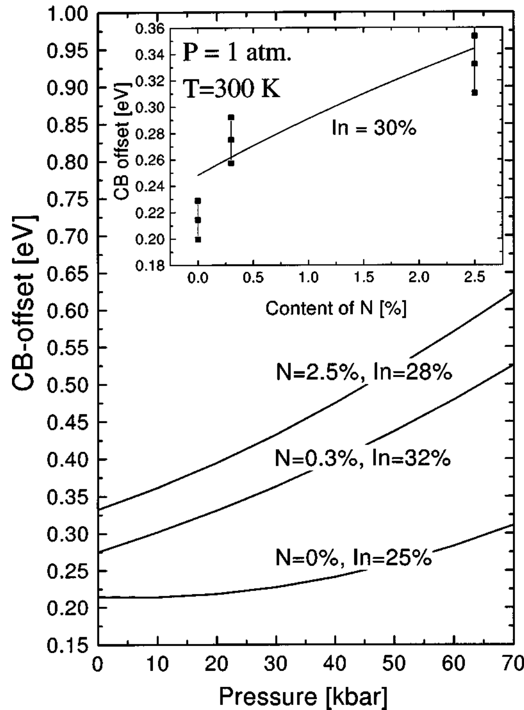

FIG. 6. Predicted pressure dependence of the $In_yGa_{1-y}As_{1-x}N_x$/GaAs CB offset for the MQW samples containing 0, 0.3, and 2.5 % N content, as calculated using the optimized ten-band $\mathbf{k}\cdot\mathbf{p}$ model. The inset curve shows the calculated effect of N fraction (to 2.5%) on the 1 atm CB offset for 30% In content. The points with error bars (reflecting uncertainty in the In and N content, Table I) are the 1 atm offsets for our specific samples.

Figure 6 gives the calculated variations of the CB offset with pressure. In the N-free sample, the offset increases because the CB edge shifts to higher energy faster in the GaAs barriers than in the $In_{0.25}Ga_{0.75}As$ wells. However, at low pressure this dependence is moderated by the effect of changes in the hydrostatic component of the mismatch strain, due to the softer compressibility of the well material relative to the barrier material. Hence, the strongest changes occur in the *quadratic* behavior above 25 kbar. The addition of N to $In_yGa_{1-y}As$ reduces its CB pressure coefficient and stiffness its compressibility. Thus, both effects are modified such that the increase in the CB offset with pressure is enhanced. This explains why the calculated increase is much stronger and begins at low pressure in the 0.3% N and 2.5% N samples. The inset to Fig. 6 shows the calculated CB offset at *ambient pressure* in the $In_yGa_{1-y}As_{1-x}N_x$/GaAs system as a function of N content. The solid curve corresponds to QWs with 30% In, and the points correspond to the specific samples studied here. The error bars indicate the possible variations in the CB offset due to the growth uncertainty in the In content. We find that the absolute value of the CB offset at 1 atm increases from 0.25 to 0.34 eV as the N content varies from 0 to 2.5 %.

The results in Figs. 5 and 6 can serve as useful guides for the engineering of infrared lasers based on $In_yGa_{1-y}As_{1-x}N_x$/GaAs which shows significantly improved optical properties for both edge-emitting and surface emitting devices compared to the $In_yGa_{1-y}As_{1-x}P_x$/InP system. The predicted increase in m_e^* and nonparabolicity with N content, which has been confirmed experimentally by several authors,[35–37] could be applied to design lasers that more nearly approach the ideal dispersion for decreased Auger recombination (realized at equal electron and hole masses[38]). Likewise, knowledge of the ability of strain to increase the CB offset in this system could be employed to reduce thermal losses, as has been done in InGaAlAs-based lasers.[39] Indeed, results on the temperature dependence of the threshold current have recently been reported for $In_yGa_{1-y}As_{1-x}N_x$/GaAs lasers, consistent with the predictions of Fig. 6.[40,41] We believe that the good fit of the present ten-band $\mathbf{k}\cdot\mathbf{p}$ model to the pressure data reported here, makes a convincing case that this model may be used as a predictive tool for the advancement of $In_yGa_{1-y}As_{1-x}N_x$/GaAs devices in the dilute-N regime.

VI. CONCLUSIONS AND SUMMARY

Photomodulated reflectance experiments under variable high-pressure and low-temperature conditions, and associated $\mathbf{k}\cdot\mathbf{p}$ calculations, have been used to investigate the influence of N on the detailed electronic structure of $In_yGa_{1-y}As_{1-x}N_x$/GaAs MQWs for $0\leqslant x\leqslant 4.3\%$. The dramatic effects of increasing N incorporation on the QW interband energies—including negative bandgap bowing, smaller total temperature variation, and strong decrease in the rate of

pressure-shift (reduced linear shifts with larger sublinear components)—are clearly illustrated by the experimental results. Our quantitative findings for the magnitude of these effects, and their variation with N content up to $x=2.5\%$, are in reasonable accord with other recent measurements and theories for III-V-N dilute alloy systems.[1,8,15–18] Moreover, the present experimental results support the importance of considering disorder in the N-cation nearest-neighbor configurations, when analyzing the interband transitions observed in quaternary QW systems. The fine structure and broadening observed in our spectral data are consistent with a weaker N-CB interaction V_{Nc} at sites having a greater number of N-In nearest-neighbor bonds, in agreement with recent suggestions of short-range bonding effects in the InGaNAs system.[25,26] The method discussed here (matching experiment with theory) also provides a predictive model of the electronic properties of $In_yGa_{1-y}As_{1-x}N_x$ structures (vs *x, y*, and strain) that can be useful for calculating laser gain and other device properties in this important infrared system. As examples, we compute the electron effective mass and the CB offset for the QW samples and pressure range studied in this work.

ACKNOWLEDGMENTS

We would like to thank Andrew Lindsay and Sandip Ghosh for useful discussions, W. Stolz for growing the samples, and EPSRC for financial support. B.A.W. wishes to thank the University of Surrey, Department of Physics, and the European Commission Research Directorate for their generous support while he was on sabbatical leave during the course of this research. P.J.K. thanks the Deutsche Forschungsgemeinschaft for financial support and E.O.R. thanks Science Foundation Ireland for financial support.

APPENDIX: DETAILED ASPECTS OF THE 10-BAND k·p CALCULATIONS

We assume that the different matrix elements in the Hamiltonian given by Eq. (1) of the text vary with N composition x and axial strain $\varepsilon_{\mathrm{ax}}$ as

$$E_{\mathrm{N}}=E_{\mathrm{N0}}-(\gamma-\kappa)x, \tag{A1}$$

$$E_{\mathrm{CB}}=E_{c0}+\frac{\hbar^2}{2m_0}s_c k_z^2-(\alpha-\kappa)x, \tag{A2}$$

$$E_{\mathrm{HH}}=E_{v0}+\kappa x-\frac{\hbar^2}{2m_0}(\gamma_1-2\gamma_2)k_z^2-\varepsilon_{\mathrm{ax}}, \tag{A3}$$

$$E_{\mathrm{LH}}=E_{v0}+\kappa x-\frac{\hbar^2}{2m_0}(\gamma_1+2\gamma_2)k_z^2+\varepsilon_{\mathrm{ax}}, \tag{A4}$$

$$E_{\mathrm{SO}}=E_{v0}+\kappa x-\Delta_{so}-\frac{\hbar^2}{2m_0}\gamma_1 k_z^2, \tag{A5}$$

$$V_{Nc}=-\beta\sqrt{x}, \tag{A6}$$

$$U=\frac{1}{\sqrt{3}}P_0 k_z, \tag{A7}$$

$$Q=\sqrt{2}\frac{\hbar^2}{m_0}\gamma_2 k_z^2-\sqrt{2}\varepsilon_{\mathrm{ax}}. \tag{A8}$$

Here $\gamma_1=\gamma_1^L-E_p/(3E_g)$ and $\gamma_{2,3}=\gamma_{2,3}^L-E_p/(6E_g)$ are Luttinger parameters $s_c=1/m^*+(E_p/3)[2/E_g+1/(E_g+\Delta_{\mathrm{SO}})]$, Δ_{SO} the spin-orbit splitting, $P_0=\sqrt{2m_0E_p/\hbar^2}$ the Kane matrix element related to the Kane energy E_p, and $\varepsilon_{\mathrm{ax}}=-b_{\mathrm{ax}}(1+2c_{12}/c_{11})\varepsilon_{xx}$ describes the effect of axial strain on the VBs, with c_{11} and c_{12} the elastic constants, b_{ax} the axial deformation potential, and ε_{xx} the in-plane strain. The parameters α and β describe the band-gap reduction due to the introduction of N, while κ takes account of the variation of the VB offset between unstrained (Ga,In)N_xAs_{1-x} and GaAs as a function of x. We set $\alpha=1.55$ eV, $\beta=1.675$ eV, $\gamma=3.5$ eV, and $\kappa=3.5$ eV, independent of strain and composition. It is assumed that the spin-orbit split-

TABLE III. Material parameters used in the present calculations to determine the $In_yGa_{1-y}As$ host band structure (scaling vs *y*), and the $In_yGa_{1-y}As_{1-x}N_x$/GaAs band alignment (scaling vs *y* and *x*). The deformation potentials a_v, and a_g, and b_{ax} are defined for hydrostatic and (001) axial strain, respectively, as in Ref. 43. All tabulated values for InN and GaN are for the zinc blende structure.

	InAs[a,b]	GaAs[a,b]	InN[c,d,e]	GaN[c,d,e]
a_0 (Å)	6.0853	5.6533	4.98	4.52
c_{11}, c_{12} (10^2 kbar)	8.33, 4.53	11.88, 5.38	18.2, 12.5	28.2, 15.9
a_v(eV), a_g(eV)	1.00, −6.08	1.16, −8.33	0.50, −3.00	0.80, −6.40
b_{ax}(eV)	−1.8	−1.7	−1.3	−1.6
E_g (eV) ($T=300$ K)	0.355	1.424		
$E_{v,\mathrm{av}}$ (eV)	−6.67	−6.92		
Δ_{SO} (eV)	0.380	0.341		
γ_1^L, γ_2^L, γ_3^L	19.7, 8.4, 9.3	6.85, 2.1, 2.9		
m^* (m_0)	0.024	0.067		
E_p(eV)	22.2	25.7		

[a]Reference 44.
[b]Reference 45.
[c]Reference 46.
[d]Reference 47.
[e]Reference 48.

ting is also independent of N content, in agreement with experiment,[1,20] and we neglect any direct N-VB coupling.[7] The inclusion of such coupling (which is predicted to be weak[7]) would introduce an additional small parameter to the calculations, whose value cannot be extracted accurately from experiment. The band-edge energies E_{CB}, E_{HH}, E_{LH}, and E_{SO} are, otherwise, assumed to have the same variations with In composition, built-in hydrostatic strain and applied hydrostatic pressure as are found in conventional $In_yGa_{1-y}As$/GaAs heterostructures.[42,43]

The N-related parameters, including $E_{N0}(P=0)$, were constrained by comparison to the tight-binding supercell calculations, and then further refined by fitting the $\mathbf{k}\cdot\mathbf{p}$ results to the interband transitions observed in the PR at 1 atm in our samples. The pressure dependence of the N level was set at $\partial E_{N0}/\partial P = 2.5$ meV/kbar. This gives a better fit to our data compared to the value of $\partial E_{N0}/\partial P = 1.5$ meV/kbar previously used in InGaAsN bulk measurements.[1] The other adjustable parameters in our calculations are the compositions and structural dimensions (nitrogen and indium content, well width, and barrier width; see Table I of the text), which are varied within the limits of growth uncertainty. We obtain the lattice constants a_0, elastic constants c_{11} and c_{12}, band-structure parameters, and band alignments (treated within the model-solid[42,43] picture) for the specific heterostructure calculations by appropriate linear scaling (quadratic scaling was used for the energy gap of host InGaAs material only) vs x and/or y of the literature values listed in Table III for the binary constituents making up the $In_yGa_{1-y}As_{1-x}N_x$ system. (See the Table III caption for more details.)

In summary a ten-band $\mathbf{k}\cdot\mathbf{p}$ Hamiltonian is used to compute the confined-state energies, and their pressure dependences, in our $In_yGa_{1-y}As_{1-x}N_x$/GaAs QW samples. The N-related energies and coupling parameters required for this model are derived by comparison to the results of realistic tight-binding supercell calculations. The use of a ten-band Hamiltonian, which explicitly includes the effects of a (spin-degenerate) N band, is essential to achieve an adequate $\mathbf{k}\cdot\mathbf{p}$ fit to the observed QW transition energies;[14] it is impossible to obtain a reasonable fit to the ground and excited transition energies using a conventional eight-band Hamiltonian.[4] There remain uncertainties in the magnitudes of the N-related parameters used in the ten-band analysis. We have shown here that it is, nevertheless, possible to derive a self-consistent set of values for these parameters. The established parameters are supported by a wide range of theoretical and experimental data, and are used here to describe ground and excited state transition energies in $In_yGa_{1-y}As_{1-x}N_x$/GaAs QWs for values of x up to 2.5%, y in the range 25–32 %, and for hydrostatic pressures to 70 kbar.

Note added. After this paper was accepted for publication two more references were added in order to clarify that the reduction of the band-gap as a function of N content in dilute N systems was already known a decade ago.[49,50]

*Email address: s.choulis@surrey.ac.uk

†Now at NMRC, University College, Lee Maltings, Prospect Row, Cork, Ireland.

‡On sabbatical at the University of Surrey, Guildford, Surrey, UK.

[1] W. Shan, W. Walukiewicz, J. W. Ager, E. E. Haller, J. F. Geisz, D. J. Friedman, J. M. Olson, and S. R. Kurtz, Phys. Rev. Lett. **82**, 1221 (1999).

[2] W. Shan, W. Walukiewicz, J. W. Ager, E. E. Haller, J. F. Geisz, D. J. Friedman, J. M. Olson, and S. R. Kurtz, J. Appl. Phys. **86**, 2349 (1999).

[3] E. D. Jones, N. A. Modine, A. A. Allerman, S. R. Kurtz, A. F. Wright, S. T. Tozer, and X. Wei, Phys. Rev. B **60**, 4430 (1999).

[4] M. Hetterich, M. D. Dawson, A. Y. Egorov, D. Bernklau, and H. Riechert, Appl. Phys. Lett. **76**, 1030 (2000).

[5] P. Perlin, P. Wisniewski, C. Skierbiszewski, T. Suski, E. Kaminska, S. G. Subramanya, E. R. Weber, D. E. Mars, and W. Walukiewicz, Appl. Phys. Lett. **76**, 1279 (2000).

[6] A. Lindsay and E. P. O'Reilly, Solid State Commun. **112**, 443 (1999).

[7] E. P. O'Reilly and A. Lindsay, Phys. Status Solidi B **216**, 131 (1999).

[8] T. Mattila, S.-H. Wei, and A. Zunger, Phys. Rev. B **60**, R11245 (1999).

[9] L. Bellaiche, S.-H. Wei, and A. Zunger, Phys. Rev. B **54**, 17 568 (1996).

[10] M. Kondow, K. Uomi, A. Niwa, T. Kitatani, S. Watahiki, and Y. Yazawa, Jpn. J. Appl. Phys. **35**, 1273 (1996).

[11] J. Hader, S. Koch, J. V. Moloney, and E. P. O'Reilly, Appl. Phys. Lett. **77**, 630 (2000).

[12] S. Illek, A. Ultsch, B. Borchert, A. Y. Egorov, and H. Riechert, Electron. Lett. **36**, 725 (2000); K. D. Choquette, J. F. Klem, A. J. Fischer, O. Blum, A. A. Allerman, I. J. Fritz, S. R. Kurtz, W. G. Breiland, R. Sieg, K. M. Geib, J. W. Scott, and R. L. Naone, *ibid.* **36**, 1388 (2000).

[13] T. Kitatani, K. Nakahara, M. Kondow, K. Uomi, and T. Tanaka, Jpn. J. Appl. Phys., Part 2 **39**, L86 (2000).

[14] S. A. Choulis, B. A. Weinstein, T. J. C. Hosea, M. Kamal-Saadi, E. P. O'Reilly, A. R. Adams, and W. Stolz, Phys. Status Solidi B **223**, 151 (2001).

[15] P. J. Klar, H. Grüning, W. Heimbrodt, J. Koch, F. Höhnsdorf, W. Stolz, P. M. A. Vicente, and J. Camassel, Appl. Phys. Lett. **76**, 3439 (2000).

[16] P. J. Klar, H. Grüning, W. Heimbrodt, J. Koch, F. Höhnsdorf, W. Stolz, P. M. A. Vicente, M. Kamal-Saadi, A. Lindsay, and E. P. O'Reilly, Phys. Status Solidi B **223**, 163 (2001).

[17] E. D. Jones, N. A. Modine, A. A. Allerman, S. R. Kurtz, A. F. Wright, S. T. Tozer, and X. Wei, Phys. Rev. B **60**, 44 430 (1999).

[18] I. Suemune, K. Uesugi, and W. Walukiewicz, Appl. Phys. Lett. **77**, 3021 (2000).

[19] F. Höhnsdorf, J. Koch, A. Hasse, K. Volz, A. Schaper, W. Stolz, G. Giannini, and L. Tapfer, Physica E (Amsterdam) **8**, 205 (2000).

[20] J. D. Perkins, A. Mascarenhas, Yong Zhang, J. F. Geisz, D. J. Friedman, J. M. Olson, and Sarah R. Kurtz, Phys. Rev. Lett. **82**, 1221 (1999).

[21] W. Shan, W. Walukiewicz, K. M. Yu, W. Ager, E. E. Haller, J. F. Geisz, D. J. Friedman, J. M. Olson, S. R. Kurtz, and C. Nauka, Phys. Rev. B **62**, 4211 (2000).

[22] D. J. Friedman, J. F. Geisz, S. R. Kurtz, and M. Olson, J. Cryst. Growth **195**, 409 (1998).
[23] S. R. Kurtz, A. A. Allerman, E. D. Jones, J. M. Gee, J. J. Banas, and B. E. Hammons, Phys. Rev. Lett. **82**, 1221 (1999).
[24] D. E. Aspnes, Surf. Sci. **37**, 418 (1973).
[25] P. J. Klar, H. Grüning, J. Koch, S. Schäfer, K. Volz, W. Stolz, W. Heimbrodt, M. Kamal-Saadi, A. Lindsay, and E. P. O'Reilly, Phys. Rev. B **64**, 121203(R) (2001).
[26] Kwiseon Kim and Alex Zunger, Phys. Rev. Lett. **86**, 1609 (2001).
[27] Sarah Kurtz, J. Webb L. Gedvilas, D. Friedman, J. Geisz, J. Olson, R. King, D. Joslin, and N. Karam, Appl. Phys. Lett. **78**, 748 (2001).
[28] S. A. Choulis, T. J. C. Hosea, P. J. Klar, M. Hofmann, and W. Stolz, Appl. Phys. Lett. **79**, 4277 (2001).
[29] A. Lindsay and E. P. O'Reilly, *Proceedings of the 25th ICPS*, edited by N. Miura and T. Ando, Vol. 87 of *Springer Proceedings in Physics* (Springer, Berlin, 2001), p. 63.
[30] M. Hofmann, A. Wagner, C. Ellmers, C. Schlichenmeier, S. Schäfer, F. Höhnsdorf, J. Koch, W. Stolz, S. W. Koch, W. W. Rühle, J. Hader, J. V. Moloney, E. P. O'Reilly, B. Borchert, A. Yu. Egorov, and H. Reichert, Appl. Phys. Lett. **78**, 3009 (2001).
[31] S. Tomić and E. P. O'Reilly, Physica E (Amsterdam) **13**, 1102 (2002).
[32] P. Perlin, S. G. Subramanya, D. E. Mars, J. Kruger, N. A. Shapiro, H. Siegle, and E. R. Weber, Appl. Phys. Lett. **73**, 3703 (1998).
[33] H. Uesugi, I. Suemune, T. Hasegava, T. Akutagava, and T. Nakamura, Appl. Phys. Lett. **76**, 1285 (2000).
[34] W. Zawadzki, Adv. Phys. **23**, 435 (1974).
[35] C. Skierbiszewski, P. Perlin, P. Wisniewski, W. Knap, T. Suski, W. Walukiewicz, W. Shan, K. M. Yu, J. W. Ager, E. E. Haller, J. F. Geisz, and M. Olson, Appl. Phys. Lett. **76**, 2409 (2000).
[36] I. A. Buyanova, G. Pozina, P. N. Hai, W. M. Chan, H. P. Xin, and C. W. Tu, Phys. Rev. B **63**, 033303 (2000).
[37] P. N. Hai, W. M. Chen, I. A. Buyanova, H. P. Xin, and C. W. Tu, Appl. Phys. Lett. **77**, 1843 (2000).
[38] A. R. Adams, Electron. Lett. **22**, 249 (1986).
[39] S. J. Sweeney, G. Knowles, T. E. Sale, and A. R. Adams, Phys. Status Solidi B **223**, 567 (2001).
[40] M. Kondow, T. Kitatani, K. Nakahara, and T. Tanaka, Jpn. J. Appl. Phys., Part 2 **38**, L1355 (1999).
[41] R. Fehse, S. J. Sweeney, A. R. Adams, E. P. O'Reilly, A. Y. Egorov, H. Riechert, and S. Illek, Electron. Lett. **37**, 92 (2001).
[42] V. A. Wilkinson, A. D. Prins, J. D. Lambkin, E. P. O'Reilly, D. J. Dunstan, L. K. Howard, and M. T. Emeny, Phys. Rev. B **42**, 3113 (1990).
[43] C. G. Van de Walle, Phys. Rev. B **39**, 1871 (1989).
[44] *Semiconductor Basic Data*, 2nd revised ed., edited by O. Madelung (Springer-Verlag, Berlin, 1996).
[45] M. P. C. M. Krijn, Semicond. Sci. Technol. **6**, 27 (1991).
[46] J. W. Orton and C. T. Foxon, Rep. Prog. Phys. **61**, 1 (1998).
[47] K. Kim, W. R. L. Lambrecht, and B. Segall, Phys. Rev. B **53**, 16 310 (1996).
[48] K. Kim, W. R. L. Lambrecht, and B. Segall, Phys. Rev. B **56**, 7018 (1997).
[49] M. Weyers, M. Sato, and H. Ando, Jpn. J. Appl. Phys., Part 2 **31**, L853 (1992).
[50] M. Weyers and M. Sato, Appl. Phys. Lett. **62**, 1396 (1993).